CHAPTER 8

Solvent Effects

This chapter provides a first attempt to deal with the environmental factors acting on POMs. In the previous chapters 4-7 we mostly studied polyoxometalates in the gas phase. Such a crude treatment is valid to study some properties but, in some cases, it may not be sufficient. The introduction of the solvent effects by means of theoretical tools has been studied for a long time. Amongst others, two theoretical approaches can be used nowadays to model the solvent effects. This chapter presents tests performed with POMs making use of a continuum model, on the one hand, and with molecular dynamics, on the other hand. In section 8.2 we discuss a few examples in which the COSMO method is utilised for recomputing the cluster energies. Section 8.3 describes the solvation of two Keggin anions treated with molecular dynamics. In this method, the solvent molecules are treated as discrete units. From this data, one can get a general picture of the disposition of water molecules around a POM.

8.1. Introduction

The results presented in previous chapters of this thesis dealt with molecules in the gas phase, just getting rid off the external factors like counterions or solvent molecules. For many considerations, it is a fairly good approximation, but for some purposes it is obligatory to go beyond this simple model, thus including the effect of the environment. Since polyoxometalates are known to exist only in solution or in crystalline matrices, an approach to reality passes through the inclusion of the molecules that surround them. Of course, the media they are in influences not only some inherent properties of POMs, but also the way they interact or react with other species. An example is the electron transfer reaction, which is discussed below. Maestre *et al.*[1] and Rohmer *et al.*[2] published the pioneering works where an external field was applied to a POM cluster. The method proposed takes into account the stabilising effects of the environment by reproducing the external potential field with a set of point charges (see chapter 3).

The aim of this chapter is to present the results obtained by using two well-known models that enable the introduction of the solvent effects to POMs. These two methodologies are briefly introduced, together with illustrative results, in sections 8.2 and 8.3. These resorts for including the environmental effects are inherently very different in their assumptions of how the solvent is treated. The information obtained from these two techniques is valuable since scarce information is available. Section 8.3 is based on unpublished results.

8.2. Solvent Treated with a Continuum Model

8.2.1. The COSMO model of solvation

When treating a solvent as a continuum material, the number of degrees of freedom associated to the solvent molecules is dramatically reduced. The computational cost of such technique is modest compared to methods that explicitly consider all molecules. The idea of approximating the solvent as a continuum material surrounding a solute molecule is ancient. Starting from the original conception of Born,[3] Kirkwood[4] and Onsager[5] for modelling the solvent at a theoretical level, countless reports inspired in those primary

approaches have been published.[6-7] In the middle 1990's, Klamt and others[8-11] applied new approaches on the definition of the molecule-shaped cavity of the solvent, thus developing a quantitative description of the solvation phenomenon. It is the so-called *conductor-like screening model* of solvation (COSMO). This model has been implemented in various programs, as in the MOPAC[12] and ADF[13] packages. The model of Klamt *et al*. assumes that a molecule in solution may be regarded as being encapsulated in a cavity surrounded by the solvent molecules. This solvent, instead of being treated as a set of discrete molecules, is viewed as constituting a continuum material with a characteristic dielectric constant, ε. The target molecule plays the role of the solute that induces a charge distribution at the surface of the continuum material, which is opposite to the charge inside the cavity. Conceptually, this charge distribution corresponds to the polarisation of the continuum material. In principle, the total charge distributed along the solvent cavity surface is equal to the charge of the molecule inside.

The model is transcribed to a mathematical expression accounting for the total electrostatic energy, expressed as

$$E^S = \int_S \sum_A \frac{Z_A \rho_S(r_S)}{|R_A - r_S|} dr_S + \int_S \int_S \frac{\rho_S(r_S)\rho_S(r_S')}{|r_S - r_S'|} + \int_V \int_S \frac{\rho(r)\rho_S(r_S)}{|r - r_S|}$$

The first term represents the interaction of the surface charges, $\rho_s(r_s)$, with the nuclei of the solute molecule, Z_A. The second term accounts for the self-interaction between solvent charges, and the third one is the electrostatic interaction of the solvent charges with the electron density of the solute, $\rho(s)$. For practical purposes, the charge distribution over the surface of the solvent cavity is depicted by discrete point charges. It is very important, in assessing the performance of the model, the level of description of the surface surrounding the solute. The fundamental approximation is to consider the cavity as the union of van der Waals (vdW) spheres centred on the atoms of the solute molecule. Connolly,[14] Gibson and Scheraga,[15] Kundrot *et al*.,[16] and Perrot *et al*.[17] have investigated the analytical properties of vdW surfaces. The basic approach consists in converting the surface of the cavity in a discrete ensemble of polyhedrons. Figure 8.1 shows the vdW surface of the Keggin anion. Some methods have been reported to reproduce this surface, although one of the most common is to generate a family of triangles, each one holding a given charge. Silla and co-

workers developed a more efficient algorithm (GEPOL) to compute the surface and volume of the cavity, with better accuracy and lower cost than Connolly's method.[18] Thus, the mathematical expression above can be reformulated in terms of this formulation.

8.2.2. Application of the COSMO to POMs

Computational details

The results showed in this section were obtained by means of the implementation of the COSMO method in the ADF program.[13] For the description of the Keggin anions, we made use of the regular TZP/STO basis sets for all atoms. The strategy conducted for obtaining the energies in solution is composed of two steps. First, geometry optimised structures were obtained in the gas phase. In a second step, single-point variational calculations were performed including the surface charges in the Fock operator self-consistently, i.e., recomputing the charges of the cavity at every SCF step. The solvent is characterised by a set of parameters. We constructed the Keggin-containing cavity with the solvent-excluding surface method, constructed by means of the GEPOL93 algorithm,[18c] in which the radius of the solvent is taken as 1.4 Å. The solvent-excluding surface converts the cusps appearing in vdW surfaces in smooth concave parts. The discretisation of the surface cavity (also know as tessellation) is also characterised by how fine the spheres are partitioned in triangles. We used a value of 5, which represents a smoother description than the default option in the ADF code. The solute is characterised by the radii of the composing atoms. In fact, the Keggin structure has only oxygens exposed to the solvent, so it is more important the choice of the oxygen radius than any other one in the framework. It is fixed at a value of 1.52 Å considering a formal charge of –2. For W^{6+} and Nb^{5+}, the radii were 1.26 and 0.78 Å, respectively. These values are taken from standard libraries of atomic data.[19] The internal atoms like P and Si do not need an accurate value of radius since they are far from interact with the solvent.

The polarisability of the continuum material is governed by its dielectric constant, ε. The value utilised for water is 78.4 and, for acetonitrile, another common solvent, it is 37.0. Provided that the COSMO equation is strictly correct for conductors, a scaling function is introduced to

the dielectric solvent-related terms. In the total energy expression for the system (solute + solvent), the factor

$$f(\varepsilon) = \frac{\varepsilon - 1}{\varepsilon + x}$$

where x is an empirical parameter, is introduced. Some authors choose x = 0.5,[8-9,11,20] whereas others take 0.0.[21-22] We utilised the latter value in our calculations.

Pye *et al*.[13] tested several ionic and neutral compounds with the various surfaces commented above, obtaining modest differences in the solvation energies for small molecules, although notably differing for large systems.

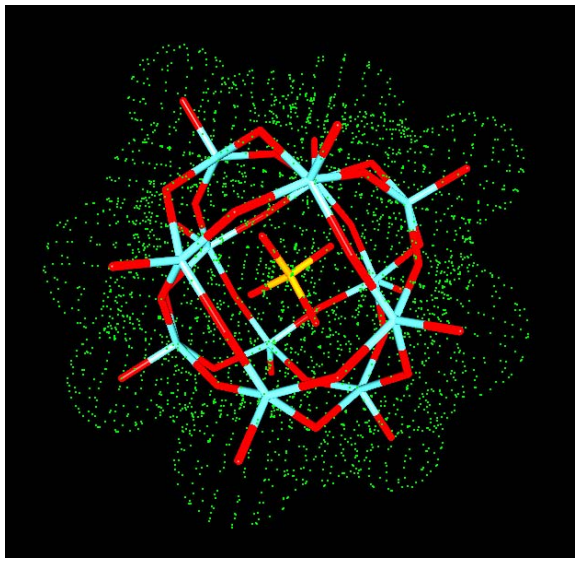

Figure 8.1. Representation of the van der Waals surface (represented as green dots) that surrounds the Keggin anion.

The electronic structure in solution

The case of POMs is especially interesting because they are, in general, molecules with a high negative charge that do not exist in the gas phase. This implies an upshift of the molecular orbital energies that is unrealistic, a

deviation being larger with the negative charge. An external field generated by the counterions and the solvent is crucial to stabilise the POMs. Therefore, for a realistic comparison of the orbital energies, the solvent has to be taken into account. In solution, many of the properties of POMs depend on the concentration, the ionic strength, the pH of the solution, etc. At present it is still not possible to take all these factors into account in a quantum chemistry study. However, a first order approximation for dilute solutions is to model the solvent effect by a polarizable continuum. The main goal of the application of the COSMO method is to put MO energies at the correct level, thus allowing the study of electron transfer reactions between POM species.

Let us take, for example, the $[PW_{12}O_{40}]^{3-}$ Keggin anion.[23] In the gas phase, the molecular orbitals are very high in energy due to the negative charge of the species. In general, POMs may be viewed as a neutral cage encapsulating an anion in its interior; this is the so-called clathrate model that allows $[PW_{12}O_{40}]^{3-}$ and $[P_2W_{18}O_{62}]^{6-}$ to be reformulated as $[PO_4]^{3-}@W_{12}O_{36}$ and $[PO_4]_2^{6-}@W_{18}O_{54}$, respectively (see chapters 1 and 4). The unoccupied metallic band of the *neutral* $W_{12}O_{36}$ and $W_{18}O_{54}$ cages appears very low in energy in the gas phase. The LUMO lies near –6.5 eV in both frameworks. The encapsulation of the phosphate anion inside the neutral cages shifts all the molecular orbitals of the POM toward higher energies. Hence, the absolute energies of the frontier orbitals in PW_{12} are +0.06 eV and +2.85 eV, respectively. When $W_{12}O_{36}$ encapsulates the SiO_4^{4-} unit, the shift is even more considerable but the H-L gap is still independent of the total charge of the encapsulated anion. Keeping in mind that POMs are *easily reducible* chemical species, the energy of the lowest unoccupied orbitals must be low enough to accept the incoming electron. The crystal field in the solid state[1] and the solvent molecules in dilute solutions stabilise the anion, and a downshift of the MOs' energies occurs. Figure 8.2 gives the orbital energies computed in the gas phase compared to those obtained including solvent effects. There is a considerable decrease in the MO energies after the solvation and the magnitude of this decrease parallels the charge of the anion. Note from those values that the LUMO and the rest of orbitals with metallic character above appear at quite negative energies after solvation (about –4 eV). This is a necessary condition for an incoming electron to be trapped in the framework.

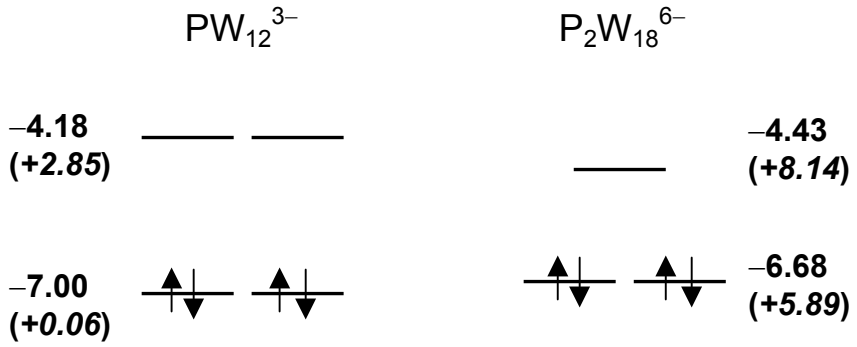

Figure 8.2. Energy of the HOMO and the LUMO for the Keggin PW_{12} and the WD P_2W_{18} anions in solution and in the gas phase (in parentheses). Values are in kcal mol^{-1}.

One goal in the introduction of the COSMO is to reproduce the correct direction of a reaction. Let us take as an example the electron transfer reaction between two POMs. It is well known that P_2W_{18}, although has a higher negative charge, is more oxidant than PW_{12}. In the gas phase, the process:

$$[PW_{12}\ 1e]^{4-} + [P_2W_{18}]^{6-} \rightarrow [PW_{12}]^{3-} + [P_2W_{18}\ 1e]^{7-}$$

was computed to be highly endothermic (ΔE = +5.07 eV) because, in absolute value, the LUMO in the WD anion lies at a higher energy. Consequently, in the absence of external fields, the extra electron simply prefers to go to the least charged PW_{12} anion. On the other hand, the frontier orbitals have similar energies in solution (Figure 8.2) and the electron transfer reaction becomes slightly exothermic (ΔE = –0.11eV), thus reproducing the experimental trend.

We also checked whether the solvent has an effect on the inner reduction properties of WD anions. The difference in stability of a P_2W_{18}1e reduced at a polar site and its partner reduced at an equatorial site is not altered by the presence of the solvent. Neither we did observe any difference in the relative stability of the reduced anions of the mixed cluster $P_2W_{15}V_3$. These results are consistent with the almost isotropic field generated by the continuum model that modifies the absolute MO energies but does not change their relative values. Therefore, in the absence of short

intermolecular contacts (such as ionic pairing or weak hydrogen bonds), the study of isolated anions suffices to understand many redox properties of POMs. Often their properties may simply be described by the electronic properties of the corresponding neutral cage. For example, the difference in the reduction energy between the polar and equatorial sites in the neutral cage $W_{18}O_{54}$ of the WD framework was computed to be 0.71 eV, a value that is very similar to the energy difference computed for the complete cluster $[PO_4]_2^{6-}@W_{18}O_{54}$, 0.84 eV.

Table 8.1. Energy change for the HOMO and LUMO for several POMs. The energy downshift fairly equalises the energy of the HOMO.

	E_{HOMO} *(eV)*		E_{LUMO} *(eV)*	
anion	$\varepsilon_o = 0$	$\varepsilon_w = 78.4$	$\varepsilon_o = 0$	$\varepsilon_w = 78.4$
$[PW_{12}]^{3-}$	0.06	–7.00	2.86	–4.18
$[PW_{12}\ 1e]^{4-}$	2.98	–6.68	5.74	–3.88
$[SiW_{12}]^{4-}$	2.99	–6.22	5.83	–3.78
$[AlW_{12}]^{5-}$	6.43	–6.26	9.24	–3.40
$[SiW_{12}\ 1e]^{5-}$	5.89	–6.43	8.70	–3.61
$[Co^{III}W_{12}]^{5-}$	5.85	–6.43	8.58	–3.65
$[AlW_{12}\ 1e]^{6-}$	9.25	–5.97	11.99	–3.17
$[Co^{II}W_{12}]^{6-}$	8.64	–6.21	11.34	–3.44
$[SiW_9Ti_3O_{40}]^{10-}$	19.36	–5.16	21.67	–2.21

Table 8.1 summarises some orbital energies of a set of polyoxoanions computed both in the gas phase and with the COSMO solvation method. The energies of HOMO and LUMO before and after inclusion of the solvent are illustrative of the effect that the COSMO has on the energy of the orbitals. The dielectric constant, ε, was chosen to be 78.4. In the gas phase, the HOMOs and LUMOs (listed in the table) are very high in energy and thus not representing realistic situations. After the COSMO calculation, the energy of the HOMOs is shifted to negative energies, which is a necessary condition for stability. Also notice that all the HOMO energies for this family of POMs lie at energies between –7 and –6 eV. This is another fact reinforcing the improvement achieved by including the external field. The

energies of the LUMOs are shifted to negative energies, as well. Taking into account that POMs are strong oxidant species, it is another necessary fact to correct in the gas-phase calculation. At the COSMO level, the energy of the LUMO allows them to accept metallic electrons and to locate them in low-lying orbitals.

However, the utilisation of this technique must be carried out with care. Some highly charged anions could be overstabilised, which could be an artefact of the model. Despite this, we claim that the study of energy reaction profiles of charged systems (see section 6.2) are realistic only if a model of solvation is taken into account.

8.3. Molecular Dynamics Simulations

8.3.1. Introduction and details of the simulations

A different point of view for studying the solvent is provided by molecular dynamics (MD). This technique does not take into account quantum considerations to study the molecular interactions. Therefore, no electron density is present and this model is not able to create or destroy bonds. It has been utilised for the study of different phenomena, such as the modelling of large ensembles of molecules. The motion of the solvent molecules can be simulated according to a standard energetic criterion and a distribution of molecules is obtained referring to their position. The information provided by MD is somewhat more qualitative than that of the COSMO model because it provides averaged statistical information although it represents in a more realistic way the behaviour of the solvent around the solute.

The solvent is not modelled as a continuum material but by a discrete ensemble of molecules in which each atom is characterised by empirical or calculated parameters. In the present case, the modelisation deals with solute molecules, as well. In the model we applied, all the molecules were left absolutely rigid, were the solvent molecules are only able to rotate and translate, whereas the solute molecule was fixed at the centre of a cell (Figure 8.3).

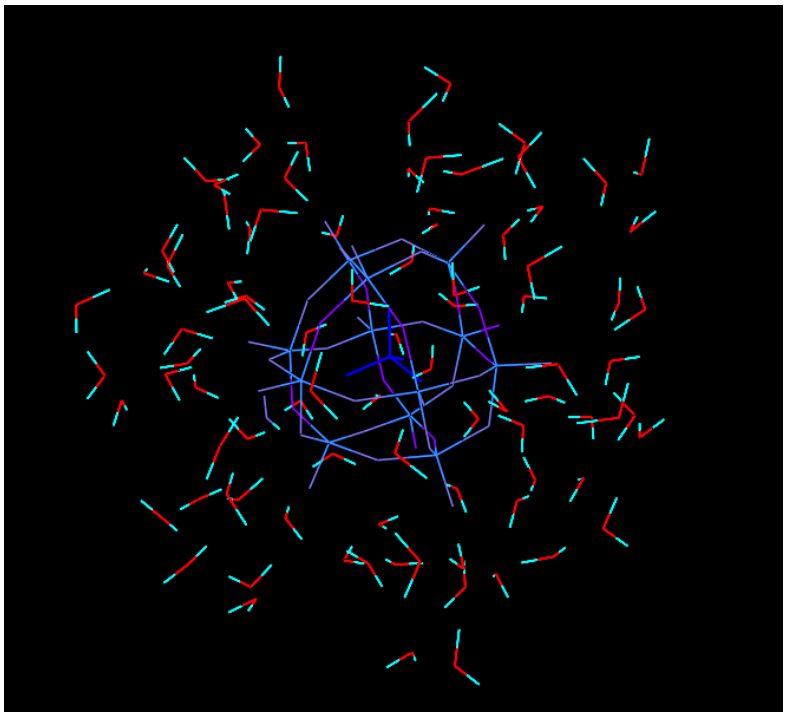

Figure 8.3. Snapshot of a molecular dynamics run. The Keggin anion is shown in blue, whereas (a few) water molecules are represented surrounding the solute molecule.

Computational details

One way for visualising the information provided by MD is to represent the *radial distribution* of the solvent molecules around the central cluster. Each MD run in the present results is characterised by the following parameters. Assuming that the total energy can be approximated by a pair-potential, we have:

$$E_{pot} = \frac{1}{2}\sum_{\substack{i,j \\ i \neq j}} \phi(r_{ij})$$

In general, $\phi(r_{ij})$ is approximated to: $\Phi(r) = \frac{\lambda^n}{r^n} - \frac{\lambda^m}{r^m}$

The van der Waals forces arising from the dipole interaction, the attractive part, corresponds to $m = 6$. The most common general potential obeys the 12-6-Lennard–Jones (LJ) potential.[24] Thus, the total potential energy is

$$\Phi(r) = \sum_i \sum_j \left(4\varepsilon_{ij} \left[\left(\frac{\sigma_{ij}}{r_{ij}} \right)^{12} - \left(\frac{\sigma_{ij}}{r_{ij}} \right)^{6} \right] + \frac{q_i q_j}{r_{ij}} \right)$$

with

$$\sigma_{ij} = \frac{1}{2}(\sigma_{ii} + \sigma_{jj}) \text{ and } \varepsilon_{ij} = \sqrt{\varepsilon_{ii}\varepsilon_{jj}}$$

In the expression of $\Phi(r)$, r_{ij} is the distance between site i and j, and q is the atomic charge, obtained by means of the Mulliken population analysis. The values of ε and σ for each element are fitted to experimental data. See Table 8.2 for a list of the parameters utilised for the MD calculations. The potential parameters for the Keggin-oxygen (water) interactions in the present calculations are:

Table 8.2. ε, σ and q parameters utilised for the molecular dynamics calculations. The atomic charges listed were calculated by Mulliken population analysis.

	ε *(kJ mol^{-1})*	σ	q	
Atoms in the Keggin			PW_{12}	$SiNb_3W_9$
P	123.45	3.000	+1.94	–
Si			–	+2.08
W	111.26	2.337	+2.85	+2.77/+2.81
Nb			–	+2.24
O_{tetra}			–0.90	–1.14
O_{bridge}	107.95	3.169	–1.06/–1.12	–0.99/–1.12
O_{term}			–0.78	–0.89/–0.91

The LJ interactions were assumed to be the same for both Keggin clusters tested (see below). The electrostatic interactions are usually much stronger than the LJ potential and the error introduced with this approximation is negligible. Since the potential decreases rapidly with r, we can apply a cut-off to the potential. For avoiding discontinuity, we choose a given value for r_0 and the termination of the potential is smoothed using a tail potential, say $\Psi(r)$ such that $\Psi(r) = \Phi(r)$ at r_0. The truncation of the forces was chosen at a cut-off intermolecular distance of 9.0 Å. The long-range electrostatic interactions were calculated by a standard Ewald summation.[25]

We constructed a (27.929 x 27.929 x 27.929) $Å^3$ cubic unit cell. The total number of water molecules inside this cage is fixed at 665. An extended simple-point-charge (SPC/E) force-field model was used for water.[26] For constructing the radial distribution curve for water, the Keggin was assumed to be spherical. The positions for all atoms of the solvent were averaged at each step of the run (excluding the positions during the equilibration time). The temperature of the experiment was fixed by means of the Berendsen thermostat[27] at 298 K, in which the instantaneous temperature is pushed towards the desired T by scaling the molecular velocities at each step of the run. The time constant was fixed at 0.2 ps. The equilibration time was fixed at 50 ps, whereas the total runtime for each experiment was 700 ps with a time step of 2.0 fs.

8.3.2. MD study of the solvation of Keggin clusters

MD calculations were carried out to obtain additional information concerning the fashion in which Keggin anions are solvated. The study was performed in collaboration with Dr. Christoph Hartnig,[28] from the Juelich Research Centre, Germany. From each MD run, the information is transformed into averaged radial distributions for the molecules of solvent around the solute anion. These curves can be plotted representing H- and O-distributions in order to identify accumulations of hydrogen or oxygen atoms of the water molecules separately. MD was used for comparing the effects of the solvent in two cases: the single-addenda $PW_{12}O_{40}^{3-}$ and the mixed-addenda $SiNb_3W_9O_{40}^{7-}$ anions. The overall charge was chosen to be different in both clusters with the aim of finding differences in the way they are solvated by water. In principle, we can expect that the solvent molecules will behave somehow differently.

MD study of $PW_{12}O_{40}^{3-}$ in water

We start the discussion of the MD results with the most symmetric single-addenda PW_{12} anion. The discussion of the results in this section is referred to oxygen positions in the Keggin anions showed in Figure 8.4.

Table 8.3. Average distances computed (in Å) from the central X atom to the terminal (O_{term}), bridging-1 (O_{brid-1}) and bridging-2 (O_{brid-2}) oxygens in PW_{12} and $SiNb_3W_9$.

	$X–O_{term}$	$X–O_{brid-1}$	$X–O_{brid-2}$
$PW_{12}O_{40}^{3-}$	5.29	3.97	3.42
$SiNb_3W_9O_{40}^{7-}$	5.52	4.10	3.40–3.59

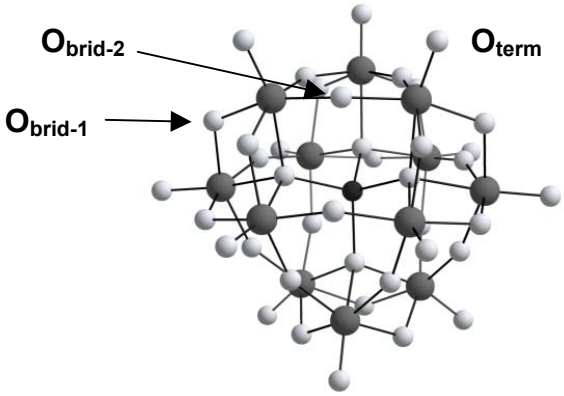

Figure 8.4. Ball-and-stick view of the Keggin anion. The three external oxygen sites are labelled.

The radial distribution of H_2O molecules around $PW_{12}O_{40}^{3-}$ is shown in Figure 8.5. Three peaks appear in the H-distribution. At distances larger than 8.6 Å from the central phosphorous, the H-distribution is almost constant indicating that the perturbations generated by the anion on the solvent are almost negligible at 4–5 Å from the Keggin surface. The first breaking of the solvent structure is found at 8.5 Å, giving rise to a band

centred at 8.3 Å and a most pronounced maximum at 7 Å. This latter peak must be mainly associated with hydrogen atoms directly interacting with terminal oxygen sites.

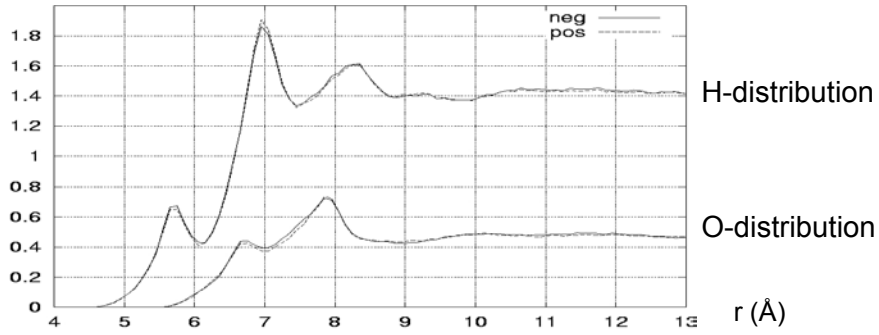

Figure 8.5. Radial distribution of H and O atoms of solvent around $PW_{12}O_{40}^{3-}$. We will discuss only de H-distribution. The origin of the x-axis is the P atom inside the Keggin. It is only represented from 4 to 13 Å, provided that at r < 4 Å we have the cluster and there are no solvent molecules.

The presence of a unique maximum in the region 7–8.5 Å in the O-distribution centred at 8 Å would indicate that both in the H-distribution belong to the same water molecule. So, the broad peak at 8.3 Å may not correspond to a H atom directly linked to one of the Keggin oxo sites. A third peak of minor intensity appears at ~5.6 Å. This accumulation must be attributed to the electrostatic interaction between the bridging sites and the water molecules. As shown in Figure 8.4, there are two distinct bridging oxygens in a Keggin framework: $O_{brid\text{-}1}$ that is at 3.97 Å from P and the more internal $O_{brid\text{-}2}$, with a P···O separation of 3.42 Å (Table 8.3). Most water molecules owning H atoms between 5 and 6 Å from the centre of the cluster would be in contact with the more external $O_{brid\text{-}1}$ oxygen, with H···O distances between 1.1 and 2 Å. The lack of a significant number of water molecules under 5 Å would be indicative of the minor accessibility of water molecules to the most internal bridging $O_{brid\text{-}2}$ oxygens. Therefore, although the two types of bridging sites have almost the same intrinsic basicity (see discussion in chapter 6) $O_{brid\text{-}1}$ and $O_{brid\text{-}2}$ would behave differently, for example, in acid-base catalysis. Taking into account that there is the same

number of terminal and O_{brid-1} sites, the affinity of water molecules for O_{term} and O_{brid-1} is approximately in a ratio 3:1. All the assignments were made taking into account a O···H distance between 1.4 and 1.8 Å. We have already mentioned in preceding chapters that terminal oxygen sites are the most exposed to the solvent molecules, which is plenty confirmed by the present MD calculations.

MD study of $SiNb_3W_9O_{40}^{7-}$ in water

The MD study of $SiNb_3W_9O_{40}^{7-}$ in a solution of water gives similar results to those found in the single-addenda anion. The radial distributions of O and H atoms of solvent were analysed making a distinction between the two *hemispheres* of the cluster: one containing the 3 Nb ions and the other only containing tungsten ions, denoted by solid and dashed lines in Figure 8.6. The larger negative charge in the Nb-derivative induces, however, some changes in the water distributions around the anion:

(i) All the peaks are shifted to smaller radial values in comparison to the distribution found for $PW_{12}O_{40}^{3-}$.

(ii) There is a new shoulder in the H-distribution, marked with an arrow in Figure 8.6, at 5 Å

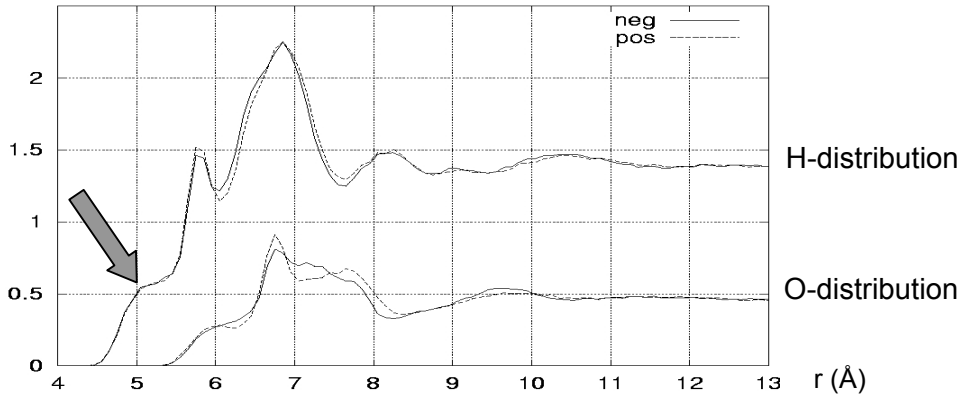

Figure 8.6. Radial distribution of H and O atoms of solvent around $SiNb_3W_9^{7-}$. The general picture resembles that of Figure 8.5, although slight changes appear.

The terminal sites keep on being surrounded by a large number of solvent molecules, but by the effect of the larger negative charge, now the local accumulation of water molecules is greater and closer to the surface of the Keggin cluster. The peak is centred at r = 6.8 Å, which means that, in average, the H···O_{term} distance is notably shorter in the substituted cluster, 1.3 Å in comparison to the value of 1.7 Å in the unsubstituted anion (see Si···O_{term} distances in Table 8.2). The number of water molecules also significantly increases in the regions near O_{brid-1} and near O_{brid-2}, as well, which is manifested by the shoulder in the H-distribution at 5 Å. Thus, we believe that this relative accumulation of water molecules would correspond to an effective interaction with the most internal O_{brid-2} site. The average H···O_{brid-2} distances are ~1.5 Å. In addition, the distribution of water molecules is almost equivalent in the two hemispheres of the anion. Despite that the negative charge is somewhat more concentrated in the Nb-region, the water molecules with the present model do not experience different forces between the *hemispheres*.

References and Notes

[1] Maestre, J. M.; Sarasa, J. P.; Bo, C; Poblet, J.-M. *Inorg. Chem.* **1998**, *37,* 3071.

[2] Rohmer, M.-M.; Bénard, M.; Blaudeau, J.-P.; Maestre, J. M.; Poblet, J. M. *Coord. Chem. Rev.* **1998**, *178–180*, 1019.

[3] Born, M. *Z. Phys*. **1920**, *1*, 45.

[4] Kirkwood, J. G. *J. Chem. Phys*. **1934**, *2*, 351.

[5] Onsager, L. *J. Am. Chem. Soc*. **1936**, *58*, 1486.

[6] Tomasi, J.; Persico, M. *Chem. Rev.* **1994**, *94*, 2027.

[7] Cramer, C. J.; Truhlar, D. G. *Chem. Rev.* **1999**, *99*, 2161.

[8] Klamt, A.; Schüürmann, G. *J. Chem. Soc, Perkin Trans*. *2*. **1993**, 799.

[9] Andzelm, J.; Kölmel, C.; Klamt, A. *J. Chem. Phys*. **1995**, *103*, 9312.

[10] Klamt, A. *J. Chem. Phys*. **1995**, *99*, 2224.

[11] Klamt, A.; Jonas, V. J. *Chem. Phys*. **1996**, *105*, 9972.

[12] Stewart, J. J. P. *QCPE Bull*. **1993**, *13*, 42.

[13] Pye, C. C.; Ziegler, T. *Theor. Chem. Acc*. **1999**, *101*, 396. ADF 2000.01. Department of Theoretical Chemistry. Vrije Universiteit. Amsterdam. Baerends, E. J.; Ellis, D. E.; Ros, P. *Chem. Phys.* **1973**, *2*, 41. Versluis, L.; Ziegler, T. *J. Chem. Phys.* **1988**, *88*, 322. Te Velde, G.; Baerends, E. J. *J. Comput. Phys.* **1992**, *99*, 84. Fonseca Guerra, C.; Snijders, J. G.; Te Velde, G.; Baerends, E. J. *Theor. Chem. Acc.* **1998**, *99*, 391.

[14] Connolly, M. L. *J. Appl. Crystallogr*. **1983**, *16*, 548. Connolly, M. L. *J. Am. Chem. Soc.* **1985**, *107*, 1118. Connolly, M. L. *J. Appl. Crystallogr*. **1986**, *18*, 499.

[15] Gibson, H. D.; Scheraga, H. A. *Mol. Phys*. **1987**, *62*, 1247. Gibson, H. D.; Scheraga, H. A. *Mol. Phys*. **1986**, *64*, 641.

[16] Kundrot, C. E.; Ponder, J. W.; Richards, F. M. *J. Comput. Chem*. **1991**, *12*, 402.

[17] Perrot, G.; Cheng, B.; Gibson, K. D.; Vila, J.; Palmer, K. A.; Nayeem, A.; Maigret, B.; Scheraga, H. A. *J. Comput. Chem*. **1992**, *13*, 1.

[18] Pascual-Ahuir, J. L.; Silla, E. *J. Comput. Chem*. **1990**, *11*, 1047. Silla, E.; Tuñón, I.; Pascual-Ahuir, J. L. *J. Comput. Chem*. **1991**, *12*, 1077. Tuñón, I.; Silla, E.; Pascual-Ahuir, J. L. *Protein Eng*. **1992**, *5*, 715. Pascual-Ahuir, J. L.; Silla, E.; Tuñón, I. *J. Comput. Chem*. **1994**, *15*, 1127.

[19] A survey of atomic data can be found in www.webelements.com.

[20] Baldridge, K.; Klamt, A. *J. Chem. Phys*. **1997**, *106*, 6622.

[21] Truong, T. N.; Stefanovich, E. V. *Chem. Phys. Lett*. **1995**, *240*, 253.

[22] Barone, V.; Cossi, M. *J. Phys. Chem. A*. **1998**, *102*, 1995.

[23] López, X.; Bo, C.; Poblet, J. M. *J. Am. Chem. Soc.* **2002**, *124*, 12574.

[24] Lennard-Jones, J. E. *Proc. Roy. Soc*. **1924**, *106*, 463.

[25] Allen, M.; Tildesley, D. *Computer Simulation of Liquids*. Oxford, **1987**. Tosi, M. P. *Solid State Physics*. Vol 16, Springer, **1964**. Kittel, C. *Introduction to Solid State Physics*. Wiley, **1986**.

[26] Berendsen, H. J. C.; Grigera, J. R.; Straatsma, T. P. *J. Phys. Chem*. **1987**, *91*, 6269. Kusalik, P. G.; Svishev, I. M. *Science*, **1994**, *265*, 1219.

[27] Berendsen, H. J. C.; Postma, J. P. M.; van Guntseren, W. F.; DiNola, A.; Haak, J. *J. Chem. Phys*. **1984**, *81*, 3684.

[28] Vassilev, P.; Hartnig, C.; Koper, M. T. M.; Frechard, F.; van Santen, R. A. *Journal of Chemical Physics*. **2001**, *115*, 9815. Hartnig, C.; Koper, M. T. M. *Journal of Chemical Physics*. **2001**, *115*, 8540.